

**DYNAMIC THERMAL TRANSPORT  
IN GRAPHENE-BASED COMPRESSIBLE FOAMS**

by  
**Zixin Xiong**

**A Thesis**

*Submitted to the Faculty of Purdue University  
In Partial Fulfillment of the Requirements for the degree of*

**Master of Science in Mechanical Engineering**



School of Mechanical Engineering

West Lafayette, Indiana

May 2021

**THE PURDUE UNIVERSITY GRADUATE SCHOOL**  
**STATEMENT OF COMMITTEE APPROVAL**

**Dr. Xiulin Ruan, Chair**

School of Mechanical Engineering

**Dr. Amy M. Marconnet**

School of Mechanical Engineering

**Dr. Xianfan Xu**

School of Mechanical Engineering

**Approved by:**

Dr. Nicole L. Key

*Dedicated to my middle school physics teacher, 唐明渝.*

## ACKNOWLEDGMENTS

It is my honor to address my gratitude to people who have offered me guidance and help in the past two years.

I deeply appreciate my advisor, Prof. Xiulin Ruan, for the opportunity to conduct research with tremendous resources. Prof. Ruan has been a patient and supportive mentor who guides me and encourages me to take challenges through my journey in academics.

I also want to thank my committee member, Prof. Amy Marconnet for her help on the experimental part of my research, and Prof. Xianfan Xu for his support.

Besides, I want to express my gratefulness to my colleagues: Prabudhya Roychowdhury, for introducing me to molecular dynamics simulations and helping with resolving my questions; Weizhi Liao, for being a great research teammate, and Albraa Alsaati and Rajath Kantharaj, for training me on infrared microscope.

For people who could not all be mentioned here, I am grateful for their feedbacks as I work through this thesis and the memory we built together at Purdue University.

# TABLE OF CONTENTS

LIST OF FIGURES .....	6
ABSTRACT.....	8
1. INTRODUCTION .....	9
1.1 Challenges in Thermal Management .....	9
1.2 Thermal Switch and Regulator .....	9
1.3 Overview of This Work .....	11
2. MOLECULAR DYNAMICS SIMULATIONS OF DYNAMIC THERMAL TRANSPORT IN COMPRESSED GRAPHENE NANOFOAMS .....	13
2.1 Simulation Setup.....	14
2.2 Simulation Process.....	14
2.3 Method Validation .....	19
2.4 Results and Discussion .....	20
2.5 Spring Model .....	22
2.6 Modified Foam.....	23
3. FINITE ELEMENT SIMULATIONS ON CONTINUUM FOAM UNIT CELL.....	25
3.1 The Continuum Model.....	25
3.2 Simulation Process.....	26
3.2.1 Mechanical Simulation .....	26
3.2.2 Thermal Simulation .....	29
3.3 Results.....	30
4. MEASUREMENTS OF VARIABLE THERMAL CONDUCTIVITY AND CONDUCTANCE OF GRAPHENE/PDMS COMPOSITE FOAM.....	32
4.1 Experimental Setup.....	32
4.2 Measuring Procedure .....	34
4.3 Results.....	36
5. CONCLUSION AND FUTURE WORK .....	39
6. REFERENCES .....	40

## LIST OF FIGURES

Figure 2.1: The side view of uncompressed and compressed domain in MD simulation. ....	13
Figure 2.2: Evolution and equilibration of simulation box dimensions in 1 <sup>st</sup> relaxation period. .	15
Figure 2.3: Temperature stays constant with fluctuation of less than 4 K while pressure increases continuously through the compression process. ....	16
Figure 2.4: Temperature rise observed in the calculation period is reduced by implementing the 2 <sup>nd</sup> relaxation period.....	17
Figure 2.5: (a) The convergence of HCACF and (b) the corresponding thermal conductivity calculation. ....	18
Figure 2.6. The calculated thermal conductivities of free-standing models are compared with reported values. The differences between two sets of data are within the range of uncertainty. .	19
Figure 2.7: (a) Thermal conductivity and (b) thermal conductance change with compressive strain in graphene random nano-foam. ....	20
Figure 2.8: The average number of neighbors of an atom increases with strain. Such increase becomes more significant with higher strain. ....	21
Figure 2.9: Schematic of the spring model. ....	22
Figure 2.10: Simulation results of thermal conductivity and thermal conductance of half-density foam up to 75% compressive strain. ....	24
Figure 3.1: SEM picture of macroscopic graphene/PDMS composite foam (left) with pore size around 200 microns and continuum porous foam frame model (right) in SOLIDWORKS.....	26
Figure 3.2: Boundary conditions for mechanical simulation.....	27
Figure 3.3: Comparison between exported model (left) and deformation result (right).....	28
Figure 3.4: Comparison between exported model with 0, 3, and 9 split planes. ....	28
Figure 3.5: Side view of exported deformed model with different strain.....	29
Figure 3.6: Thermal boundary loading. ....	29
Figure 3.7: Temperature gradient obtained in thermal simulation on uncompressed frame model. ....	30
Figure 3.8: Simulation results with spring model prediction.....	31
Figure 4.1: SEM photos of graphene/PDMS flexible foam.....	32
Figure 4.2: (a)(b) Experiment setup and (c) sandwiched sample. ....	33
Figure 4.3: (a) IR microscope focus image, (b) emissivity calibration map, and (c) temperature map. ....	35

Figure 4.4: (a)1D temperature profile and (b) 2D temperature map with corresponding regions.	36
Figure 4.5: Temperature drop at various heat flux of foam with different thicknesses. ....	37
Figure 4.6: Variation of thermal conductivity of graphene/PDMS foam with compressive strain. .....	38

## ABSTRACT

Thermal management of many electronic devices is challenged by their strict optimal operating temperature range, various operation modes, and extreme environmental conditions. The design of thermal switches and thermal regulators provides possible solution. A thermal switch with high switching ratio can be an efficient conductor that dissipates heat to avoid overheating and an insulator that protects the device from degradation and damage due to low environment temperature. A thermal regulator offers continuous tuning between maximum and minimum conductance/resistance. Graphene-based compressible foams are studied in this work as a potential material in all-solid-state thermal switch/regulator with dynamic tuning. Molecular dynamics simulations are performed on graphene nanofoams to provide insight on thermal behavior under compressive loading. The switching ratio in the cross-plane thermal conductance reaches 4.6 from 25% to 60% strain. We find that, unexpectedly, the thermal conductivity decreases as the strain increases (i.e., density increases) in low strain region. This is explained using a 1D spring model, whose thermal conductance remains constant with increasing strain if no internal contact is made in the spring and therefore, the cross-plane thermal conductivity decreases. The compressible foam structure is further studied in a continuum model, again confirming the behavior of the spring model. The strain-tuned thermal properties of macroscopic graphene/PDMS composite foam are then measured using infrared microscope. It is observed that such properties are more sensitive to strain at high compression level which confirms the MD simulation results.



# **1. INTRODUCTION**

## **1.1 Challenges in Thermal Management**

The advance in innovative electronic technology and replacement of traditional mechanical systems by compact digitally controlled electric systems lead to rapid escalation of the number of electronic devices and the fields of their application. The demand in thermal management solutions under various operation scenarios, as a result, increases and has driven the research and technology development in heat transfer community for decades. Many electronic devices require an optimal range of operating temperature to reach high performance. A temperature beyond the range of optimal performance or safe operation can cause a reduction in efficiency or permanent damage to the system, respectively. Lithium-ion battery, for instance, is a widely used rechargeable source of energy for portable electronic devices and electric vehicles. Optimal operation can be achieved between 25 °C and 40 °C [1]. The lifespan and charging efficiency reduce significantly at high battery temperature above 50 °C [2]. Thermal runaway occurs from 70 °C to 100 °C, resulting in battery safety issues [3]. On the other hand, under sub-zero conditions, problems of loss in energy and power capability as well as battery degradation also need to be resolved [4]. A desired operating temperature range for electric vehicle battery packs is from 15 °C to 40 °C for best performance and long life cycle [5]. Hence, the heat generated by the battery due to power loss during operation needs to be dissipated effectively at high ambient temperature and, in contrast, may need to be retained to keep the battery warm in cold environment.

## **1.2 Thermal Switch and Regulator**

The required change in heat dissipation rate can be achieved by establishing and breaking the thermal pathway between two contacts by a thermal switch. When a thermal switch is at “ON” state, the thermal contact is made, and high thermal conductance is measured between two contacts. At “OFF” state, the contact breaks, and thermal conductance is minimized. Thermal switch designs have been proposed with a variety of materials for one or more desired properties: high switching ratio, fast switching speed, scalability, unique triggering mechanisms, and potential applications. Cho et al. [6] has decreased the thermal resistance between two moving Si plates from 40 K/W to 2 K/W by forming arrays of liquid-metal micro-droplets with diameter of 30 microns on the base

plate at “ON” switching state. To ensure reasonable conduction at “OFF” state, pressurized air is filled between the plates as working fluid. The achieved thermal resistance ratio between “OFF” and “ON” state is 129. The contact is made and broken by adjusting the position of the top Si plate. Similar triggering mechanism is used by Gu et al. [7] in a three-slab near-field radiative thermal switch. Radiative heat flux in the system varies from 7500 to 32000 W/m<sup>2</sup> by moving the Vanadium dioxide (VO<sub>2</sub>) film between two SiO<sub>2</sub> plates at different temperature. VO<sub>2</sub> is an insulator-metal transition material whose optical properties change with small variation of temperature around its critical point. In many applications, especially for compact devices, the space available for implementation of moving mechanism is limited. In another design with liquid metal droplet by Yang et al. [8], the thermal switch is triggered by rolling the droplet in and out of position in a sealed channel to connect and disconnect the pathway between hot and cold reservoirs. The maximum reported thermal resistance ratio is 71.3. There are also applications in larger length scale, for instance, in electric vehicle battery thermal management. Hao et al. [9] controls the touching and non-touching of an interface gap between commercial 18650 Li-ion battery cells and heat sink by shape memory alloy, and demonstrates thermal conductance switching from 1.13 Wm<sup>-2</sup>K<sup>-1</sup> to 2340 Wm<sup>-2</sup>K<sup>-1</sup>. Other researchers are inspired by DNA sequences to design a biosynthesized material with predicted switching ratio of 4.5 through hydration and dehydration [10].

Some applications require thermal management that offers more precise control than two distinguish states in thermal switches. A thermal regulator provides continuous tuning on thermal conductance that maintain the device temperature within desired range. Chang et al. [11] proposed a micro-scale multiwall carbon nanotube thermal switch/regulator which displays an exponential dependence of thermal resistance on sliding distance of outer shell with respect to the inner core. The total resistance switching ratio reaches 6 at a sliding distance of 300 nm. The switching ratio progresses slowly to 1.5 till 250 nm, and aggressively increases to 6 from 250 nm to 300 nm. Since the resistance tuning between 1.5 and 6 is difficult to control precisely, the system behaves more like a thermal switch. The non-linearity in resistance tuning is one of the challenges in designing thermal regulator and requires careful characterization.

The design criteria among thermal switches and regulators include fast switching/regulating response, simple triggering mechanism, reliable material, and high switching ratio. Graphene, a two-dimensional sheet composed by carbon atoms in hexagonal lattice bonded by sp<sup>2</sup> bonds, has

been intensely studied since its discovery due to its superior thermal conductivity reported from 3000 to 5300  $\text{Wm}^{-1}\text{K}^{-1}$  [12] [13]. Chen et al. [14] fabricated three-dimensional graphene foam using chemical vapor deposition method. Li et al. [15] reported thermal conductivity of graphene foam to be  $\sim 0.3 \text{ Wm}^{-1}\text{K}^{-1}$  at room temperature. Graphene foam has been considered as the filler that enhances thermal transport properties of polymer composites [16] [17]. Thermal conductivity of GF/PDMS composite is further improved by Zhao et al. [18] [19] to  $0.56 \text{ Wm}^{-1}\text{K}^{-1}$  and  $1.08 \text{ Wm}^{-1}\text{K}^{-1}$  with carbon fiber and multilayer graphene flakes, respectively. If the foams are flexible, thermal switching may be achieved by compressing the foams, but it has not been previously pursued for thermal switching functionality yet. This motivates us to study graphene-based compressible foam in this work as a potential material of thermal regulator with tunable thermal conductivity and conductance.

### 1.3 Overview of This Work

In this work, both simulations and experiments are conducted to study the tuning curve of thermal conductivity and conductance of graphene-based compressible foams. Molecular dynamics (MD) simulations are first performed on a cubic pure graphene random nano-foam model with similar topology as graphene foam fabricated by coating on Ni base frame but with a smaller scale. The system is compressed uniaxially, and equilibrium molecular dynamics method is used to calculate the thermal conductivity of the system at 300 K. The model is later modified by removing half of the atoms within the system to understand thermal behavior of a structure of less mass density. Secondly, the relation between thermal conductance and strain is simulated using finite element method on a continuum model. Such relation is then observed and measured in graphene/PDMS flexible foam through an infrared microscope. These three systems of study differ significantly in dimensions, geometry, and therefore, magnitude of thermal conductivity and conductance. However, they share the same underlying physics. To compare across three subjects, a unitless property fraction is introduced as:

$$r_{x,i} = \frac{x_i}{x_o}, \quad (1.1)$$

where  $x$  represents the thermal property of interest, i.e., thermal conductivity  $k$ , thermal conductance  $G$ , and thermal resistance  $R$ , and  $i$  is the compression state at which the property is compared with that at  $o$ , the uncompressed natural state. When  $i$  is the state with maximum strain

that can be achieved by the system or the experiment apparatus,  $r_{x,i}$  is the switching ratio of the system, considering it as a thermal switch with only “ON” and “OFF” states.

## 2. MOLECULAR DYNAMICS SIMULATIONS OF DYNAMIC THERMAL TRANSPORT IN COMPRESSED GRAPHENE NANOFOAMS

Molecular dynamics (MD) simulation traces the evolution of a system due to user defined stimulation (i.e., thermal and mechanical loads) during a period of time by solving Newton's equation of motion. It allows the user to capture the velocity and position of each particle defined in the model, by carefully defining the interacting forces among particles and time interval between calculations of particle trajectory. It is an effective tool for studying dynamic systems. We expect to gain critical insights on thermal behavior of compressible graphene-based foam in nanoscale and the mechanism that causes such unique behavior.

The MD simulations are performed using Large-scale Atomic/Molecular Massively Parallel Simulator (LAMMPS) [20] on Purdue's research computer cluster. The uncompressed graphene nano-foam structures are adopted from Ref. [21] as provided by Dr. Pedrielli. The modeling process is inspired by the fabrication of macroscopic free-standing graphene foam by coating graphene on metallic scaffold using CVD method. A single layer graphene film is formed on a random base structure that is later removed. The side view of the atomic structure is shown in Fig. 2.1 using VMD [22]. Thermal conductivity is determined in equilibrium MD simulation using Green-Kubo approach [23] [24].

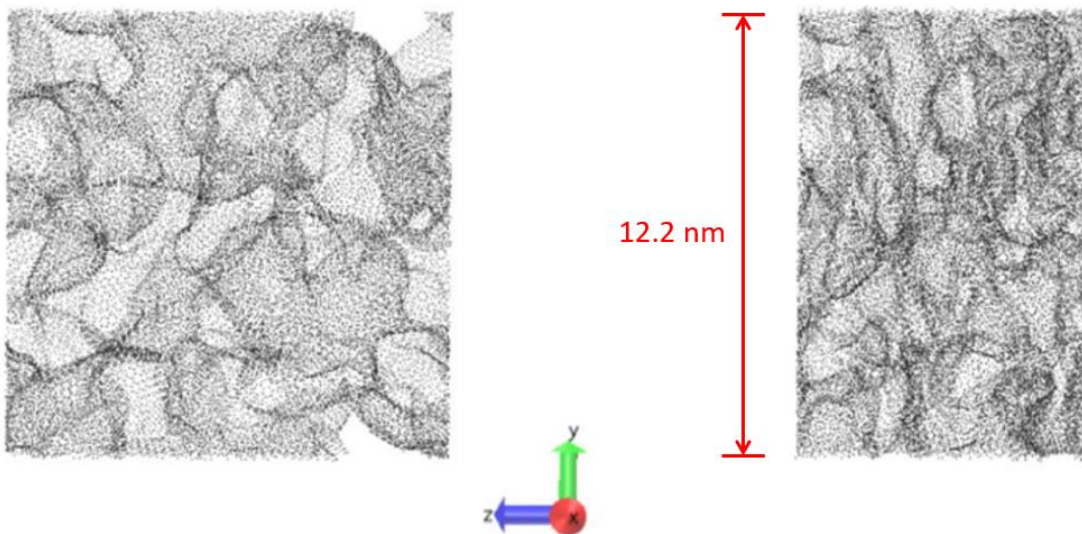


Figure 2.1: The side view of uncompressed and compressed domain in MD simulation.

## 2.1 Simulation Setup

The position of each carbon atom and simulation box dimensions are extracted from the shared models and then compiled into a formatted file according to requirement of “atomic” style in LAMMPS. The adequate atomic mass is also assigned in this file. Periodic boundary condition is applied in all directions to eliminate boundary effects and allow the results to represent the situation in a larger scale. The timestep is set to be 0.5 fs. Since the foam model is flexible and random motion of foam branches is observed even when no load is applied, a small timestep of 0.5 fs is set to carefully trace the evolution of atoms and regulate fixed variables in each simulation ensemble. The interaction between carbon atoms is modeled via the Tersoff potential for each atom [25]. Tersoff potential is a multi-body potential that include local environment effects on C-C bonds. The total force acted on a carbon atom depends on the number of neighboring atoms. Tersoff potential accurately reflects the interatomic forces in system of this work in which atoms are squeezed closely together at high compressive strain. Tersoff potential is implemented using “pair\_style” command.

## 2.2 Simulation Process

The simulation is performed in four steps. The first step is to relax the system and minimize the total energy. Two typical ensembles for system equilibration are isothermal-isobaric (NPT) and canonical (NVT). They both maintain a fixed total number of atoms and system temperature. The NVT ensemble also controls the volume of the simulation box, while the NPT ensemble allows the system to expand and shrink with certain pressure applied (0 pressure during system equilibration). The time needed before system equilibrium in NPT ensemble is usually longer due to variation in system dimensions, especially for system with low bonding strength and little interconnection support. Even though, for the flexible foam model, NVT ensemble will stabilize the system faster, the system should be allowed to achieve its relaxed dimensions as a free-standing foam model subjected to no pressure load. Hence, NPT ensemble of 50 ps is used for system relaxation at 300 K. A uniform system expansion and convergence are observed in the first 5 ps shown in Fig. 2.2. The fluctuation in temperature and total energy stabilize and the system reaches equilibrium by the end of this period.

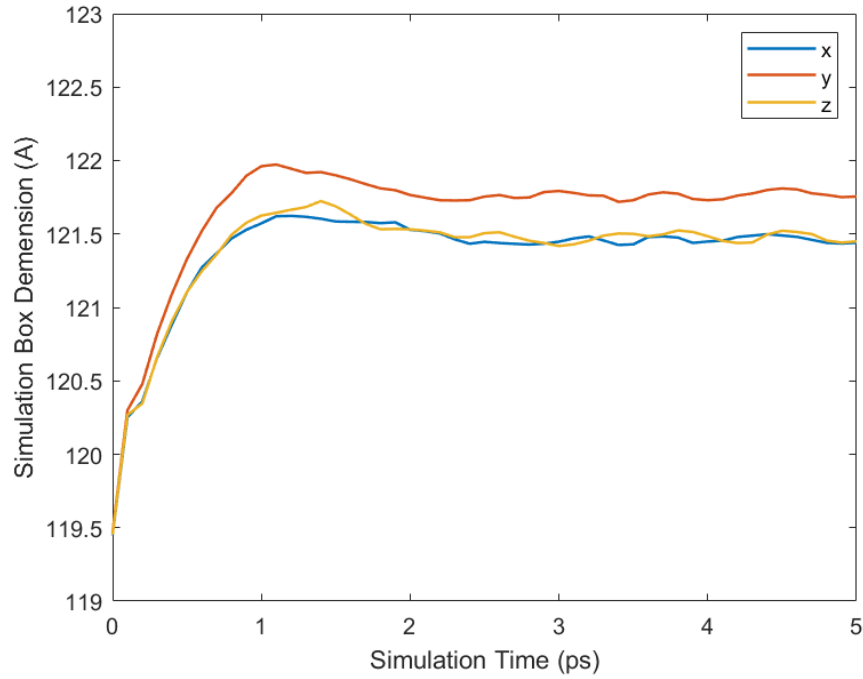


Figure 2.2: Evolution and equilibration of simulation box dimensions in 1<sup>st</sup> relaxation period.

The stabilized system is then uniaxially compressed in z-direction to desired thickness while maintaining the same thickness in x and y-directions. The compression process is achieved by using the “fix deform” command in LAMMPS which recalculates the atom position according to changes in dimensions of the simulation box. This step is performed in NVT ensemble at 300 K. Shown in Fig. 2.3, the temperature is maintained relatively constant due to small variation in kinetic energy of atoms, since the “fix deform” command only remaps the coordinates of each atom and does not introduce velocity to atoms when moving them to their new positions. The potential energy, on the other hand, increases due to more compulsion occurred within the compressed system, resulting in an increase in total energy of the system.

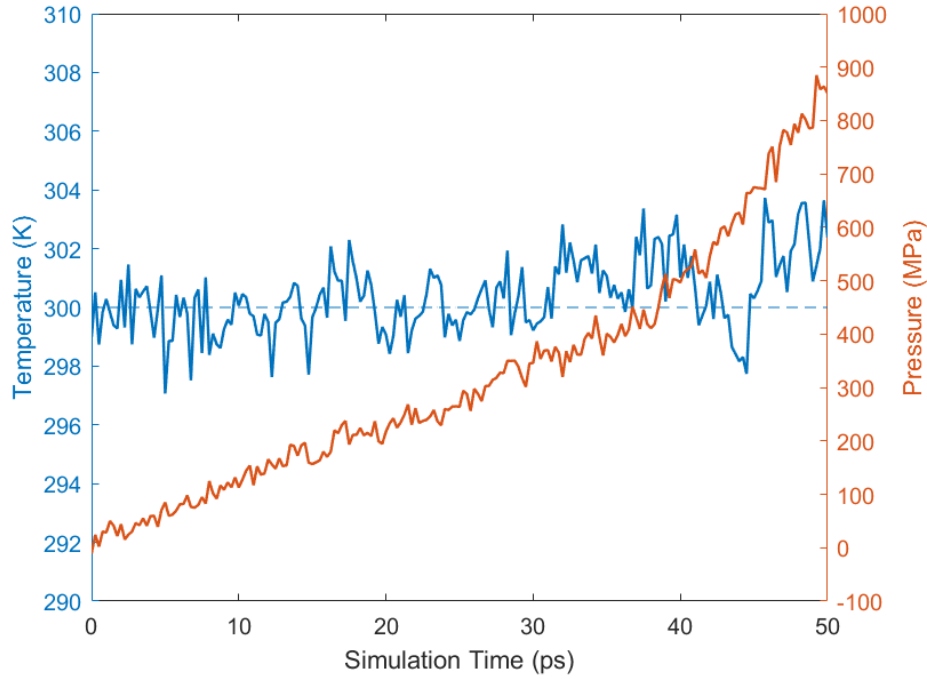


Figure 2.3: Temperature stays constant with fluctuation of less than 4 K while pressure increases continuously through the compression process.

Following the compression step is the second relaxation period. This step was not implemented in the first several simulations based on the assumption that the system is near equilibrium after compression since the compressive strain was applied slowly and at constant temperature. However, during the thermal conductivity calculation using Green-Kubo method after compression, a temperature rise was observed. Foam with larger mass density, i.e., smaller thickness, has a higher rate of temperature increase. The system could be unstable after rescaling the position of atoms. Since total energy is conserved calculation step, some potential energy converts into kinetic energy which leads to a rise in temperature. A relaxation period of 100 ps is therefore introduced, allowing the atoms to move to locations that minimize the total energy of the system. Unlike in the equilibration performed at the beginning where the volume of the simulation box is subject to change, dimensions of the system are fixed at values obtained at the end of the compression period. The equilibration temperature is kept at 300 K as in previous steps. By implementing the second relaxation period, the temperature rise in the last calculation period is reduced, as shown in Figure 2.4, especially for cases with large compression strain. According to Li et al.'s study on temperature dependence of macroscale free-standing graphene foam, its thermal



conductivity increases with temperature above room temperature. The percentage of increase below 350 K, however, is less than 1.5% [26]. Hence, the error in thermal conductivity calculation due to temperature rise is small when it is kept below  $\sim 310$  K by the second relaxation period.

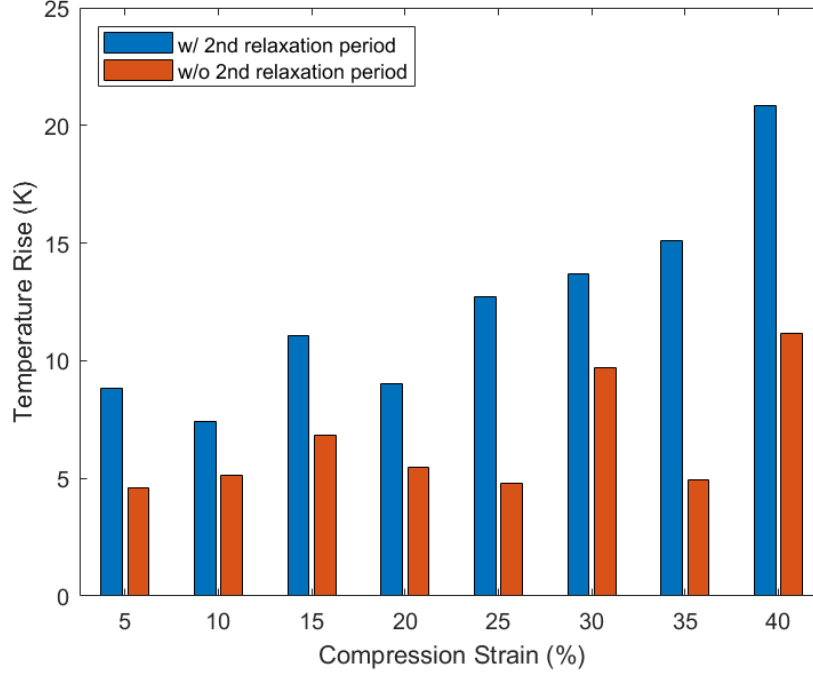


Figure 2.4: Temperature rise observed in the calculation period is reduced by implementing the 2<sup>nd</sup> relaxation period.

The last step is the calculation of thermal conductivity. Two methods commonly used for thermal conductivity calculation in MD simulation is NEMD and EMD. The NEMD method determines thermal conductivity in the direction of applied heat flux based on the resultant temperature gradient using Fourier's Law. The EMD method obtains thermal conductivity in all directions of an equilibrated system with uniform temperature by calculating the heat current auto-correlation function (HCACF). To efficiently study the in-plane and cross-plane thermal behavior of compressed foam, EMD Green-Kubo method is used [23] [24]. The heat current can be expressed as:

$$\vec{J} = \frac{1}{V} \left( \sum_i E_i \vec{v}_i + \frac{1}{2} \sum_{i < j} (\vec{F}_{ij} \cdot (\vec{v}_i + \vec{v}_j) \vec{r}_{ij}) \right), \quad (2.1)$$

where  $V$  is the volume of the system,  $E$  is the total energy per atom,  $v$  is the velocity of atom  $i$ ,  $F$  is the pair-wise force between atom  $i$  and  $j$  obtained by interatomic potential, and  $r$  is the distance

between two atoms. The time integration of HCACF is determined by the “trap” function, using trapezoidal rule. The thermal conductivity at temperature  $T$  is calculated as:

$$k = \frac{V}{3k_B T^2} \int_0^\infty \langle \vec{J}(0) \cdot \vec{J}(t) \rangle dt, \quad (2.2)$$

where  $k_B$  is the Boltzmann constant, and  $t$  is the correlation time with respect to which the HCACF is integrated. To implement Green-Kubo method in MD simulation, the calculation is performed in microcanonical ensemble (NVE). The heat currents in three directions are calculated based on kinetic energy, potential energy, and stress per atom. The auto-correlation function is sampled every 10 timesteps. The time interval between two correlation points is a multiple of 1000. The average of heat current is calculated every 10000 timesteps. Shown in Fig. 2.5a is the convergence of HCACF. Figure 2.5b shows the evolution of calculated directional and average thermal conductivity. At 400 ps, the calculation converges.

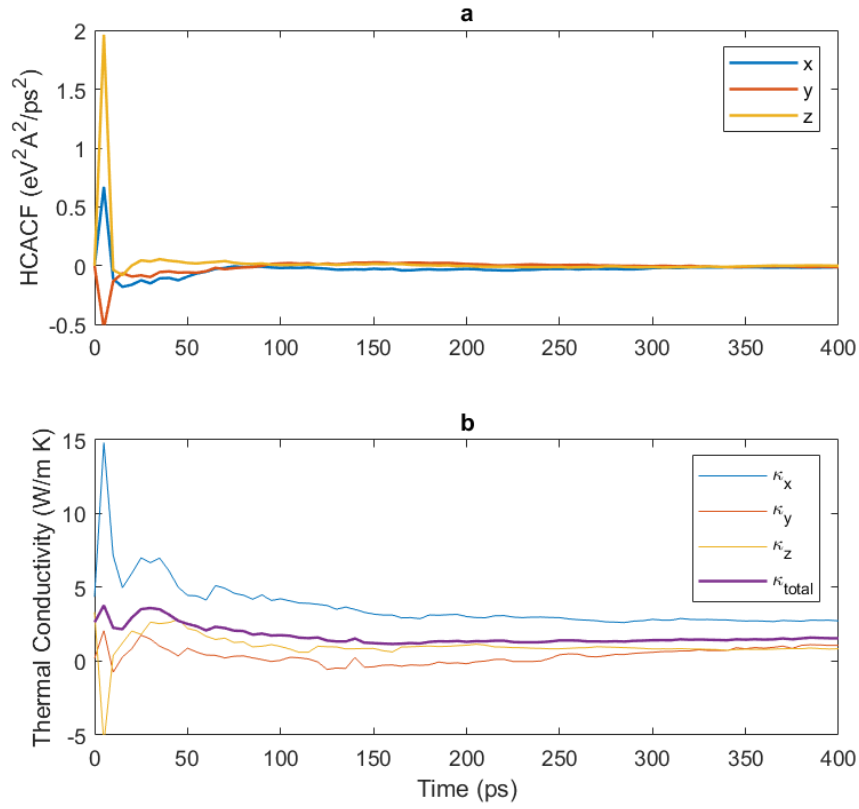


Figure 2.5: (a) The convergence of HCACF and (b) the corresponding thermal conductivity calculation.

### 2.3 Method Validation

There are four graphene random nano-foams with different mass densities. Before applying strain to the system, the simulation method is validated by comparing results on free-standing foam models. The comparison is shown in Fig. 2.6. The simulation results are similar to those reported in Ref. [21]. The difference grows for models with higher mass density. There are more atoms in the simulation box with the same dimensions for foams with high mass density, and the system requires a longer relaxation time to approach equilibrium state.

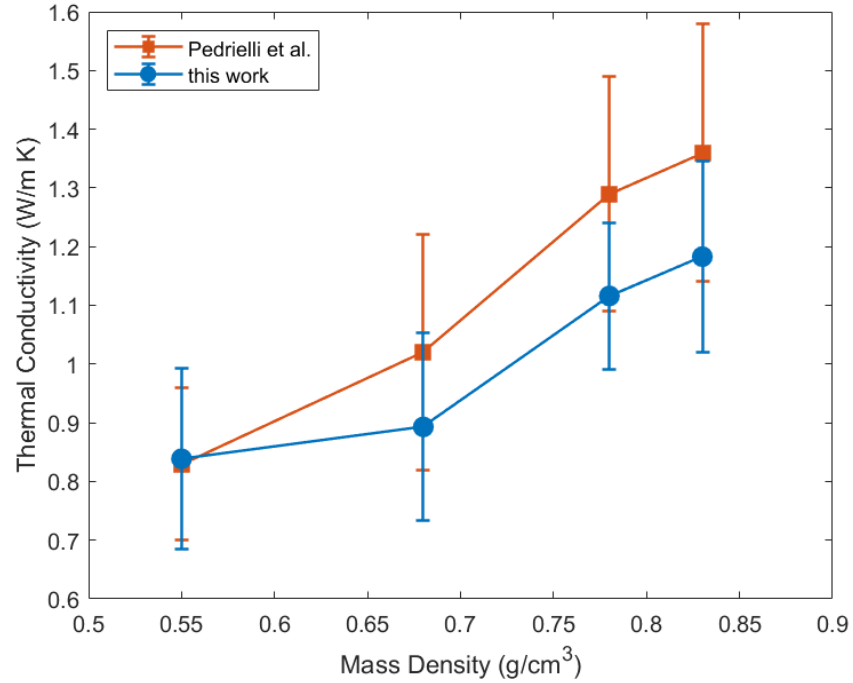


Figure 2.6. The calculated thermal conductivities of free-standing models are compared with reported values. The differences between two sets of data are within the range of uncertainty.

The system is assumed at equilibrium after the second relaxation period. However, there are still some random motions of atoms within the system and more of such random motions are in systems with larger number of atoms. On a larger scale, the movement of foam branches is also observed during the calculation period. According to the modeling method, graphene is coated on a base structure and forms a film-like structure after the base is removed. Despite the vibration around equilibrium position due to bonding between the neighboring atoms, the atoms together as a hanging branch in the empty space within the foam. Unlike a solid crystal, the foam is soft and flexible, which is an advantage and the reason why it is chosen as the subject of interest to study.

Such characteristic enables the structure of the foam to change with little stimulation. The changes in the structure have significant impact on thermal properties of the system including thermal conductivity. Therefore, the movement of foam branches introduces calculation uncertainty. The difference between calculated and reported data is within the uncertainty range of both data sets, and the simulation method is validated.

## 2.4 Results and Discussion

A maximum compressive strain of 60% is applied to the model with an increment of 5% strain. The calculated directional and average thermal conductivities at each thickness are plotted in Fig. 2.7a. The in-plane thermal conductivities stay relatively constant until it reaches 25% strain. They then start to increase with larger strain applied. The cross-plane, on the other hand, shows a decrease before 45% strain and an increase afterwards. The average thermal conductivity, as a result, decreases in low strain region and increases in high strain region. Such decrease is not expected since the mass density increases with increasing strain and thermal transport should be more efficient as more thermal pathways are available at high mass density. In Ref. [21], the thermal conductivities of four different foam models also increase with mass density. It can also be concluded from the evolution of directional thermal conductivities that the foam becomes anisotropic with strain.

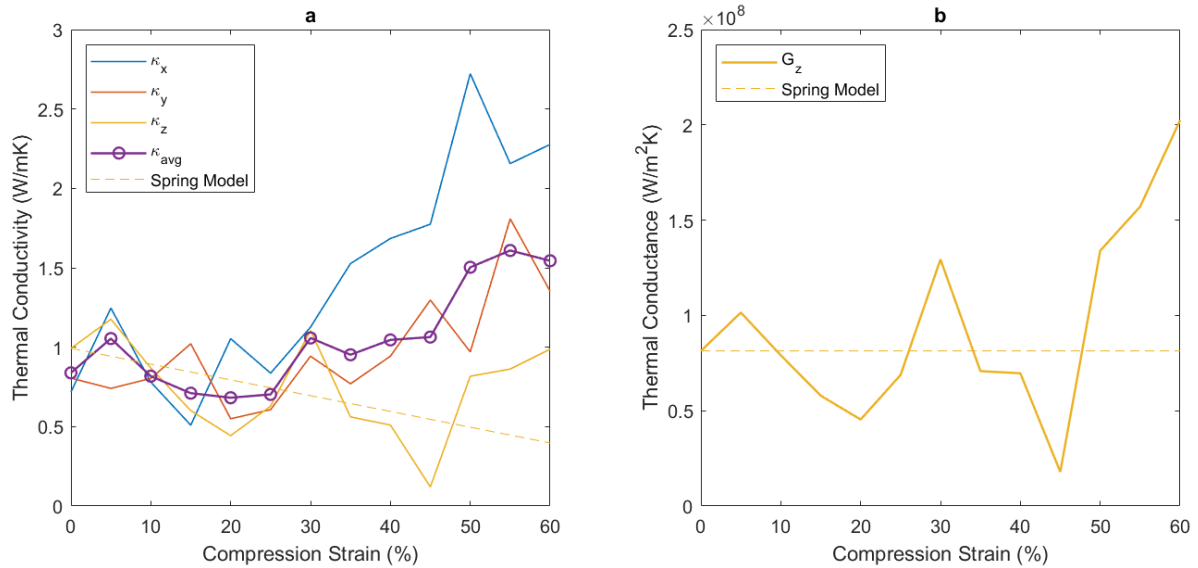


Figure 2.7: (a) Thermal conductivity and (b) thermal conductance change with compressive strain in graphene random nano-foam.

Beyond 25% strain, as more compressive strain is applied to the foam, less cavity is left in the foam and the branches start to make more contact with each other. The average number atoms within the cutoff radius among all particles in the system is found to increase with strain. An increase in the number of neighbors to each atom results in more interactions between atoms and creates more pathways for heat transfer. The percentage increase in average number neighboring atoms is plotted in Fig. 2.8. A more significant growth is found at high strain level, corresponding to more rapid increase in in-plane thermal conductivities.

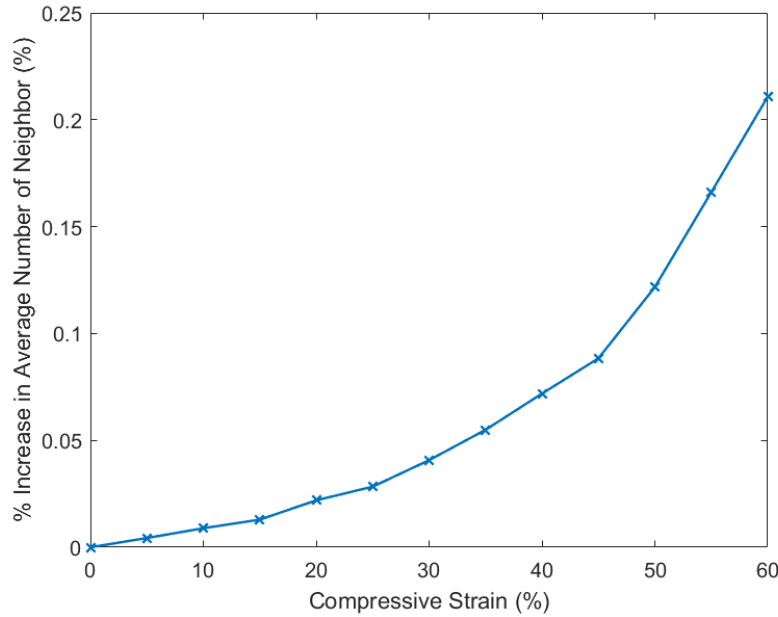


Figure 2.8: The average number of neighbors of an atom increases with strain. Such increase becomes more significant with higher strain.

Even though, larger mass density results in higher thermal conductivities [21], the change in thermal conductivity of compressed foam is more dramatic, especially for cases beyond 45% strain. This is because the internal contact in free-standing foams does not increase with mass density, since the foam is modeled in a way that a single layer of carbon atoms is coated on the base frame that eliminates internal contact. In compressed foam, however, graphene foam branches are forced to be in contact, which creates more thermal pathways for heat transfer.

## 2.5 Spring Model

To explain the counter-intuitive behavior of the foam in low strain region, a spring model is proposed by modeling the 3D foam as a 1D spring with total length  $L$  between two plates at different temperatures, shown in Fig. 2.9. Assuming the material of the spring has thermal conductivity  $k_m$  and the effective thermal conductivities between two plates in uncompressed and compressed states are  $k_u$  and  $k_c$ , respectively. The thermal conductance in uncompressed and compressed states can be expressed as:

$$G_u = \frac{k_u A_s}{x_u} = \frac{k_m A_m}{L}, \quad (2.3)$$

$$G_c = \frac{k_c A_s}{x_c} = \frac{k_m A_m}{L}, \quad (2.4)$$

where  $A_s$  is the cross-section area of the spring,  $A_m$  is the cross-section of the wire, and  $x_u$  and  $x_c$  are the distance between two plates in uncompressed and compressed states, respectively. Since the length of the pathway that heat flows through in both cases is the length of the wire of the spring, thermal conductance stays constant as the spring being compressed, while the effective thermal conductivity between two plates decreases due to a smaller distance  $x_c$ . The predicted thermal conductivity by spring, therefore, decreases with increasing mass density. However, if the distance of the pathway traveled through by heat decreases, i.e., ligaments or branches make contact in a compressed foam, heat transfer between hot and cold reservoirs becomes more efficient, which leads to higher thermal conductance.

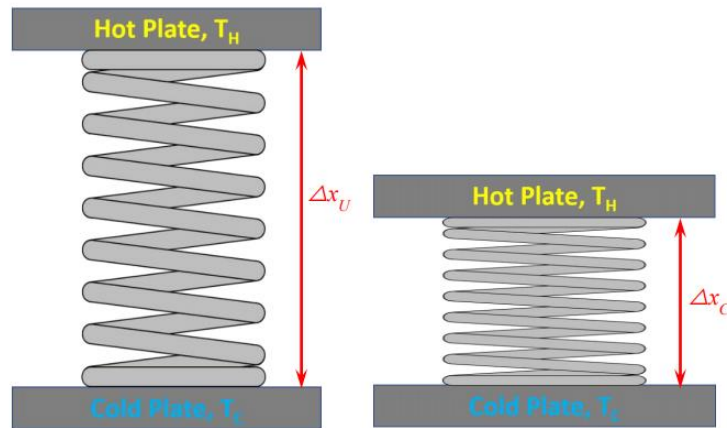


Figure 2.9: Schematic of the spring model.

The prediction of thermal conductivity and conductance based on spring model is plotted in Fig. 2.7 as dash lines. The spring model accurately reflects the thermal conductivity behavior of the foam in cross-plane direction at low strains where internal contact is negligible due to low strain. As high strain is applied, more contact is made between foam branches which dominates change in thermal conductivity and conductance.

## 2.6 Modified Foam

Among four models of graphene random nanofoam, the initial decreasing trend described by the proposed spring model is less significant in foam with high mass density since internal contact is easier to establish when the foam is more compact initially. To study the dynamic behavior of a less dense foam with higher maximum possible compressive strain, a modification is applied to the foam model with lowest mass density among four models, by manually remove half of the atoms. The simplest way to remove half of the atoms is applying a random selection by atom index. This approach, however, creates defects in the hexagonal graphene structure. To maintain a similar foam geometry as the original foam model, the atoms are removed from the tips of hanging branches, leaving some branches unchanged. The operation is performed in VMD [22].

The same method in equilibrium MD simulation is used to calculate the thermal conductivity as for the original foams. Since the mass density is cut in half, a larger strain can be applied to the system without causing significant stress in the model that damages the structure and induces calculation error due to unstable system. The foam is compressed to 25% of its original thickness with an interval of 5%. The results are plotted in Fig. 2.10. A decrease in thermal conductivity is observed below a strain of 60%, while a slight increase occurs afterwards. The instability of the system lead to high calculation uncertainty. After half of the atoms are carefully removed from the original model, there are broken branches floating in the system, resulting in a different foam structure every timestep. It is visualized using VMD that the movement of branches is at a higher extent, creating more error in the thermal conductivity calculation. As the foam is compressed below 40% of its original thickness, more branches are in contact, and less space is left for hanging branches to move freely. The system becomes more stable at high mass density states. Similar to the case of original foam models, an increase in the number of neighboring atoms occurs.

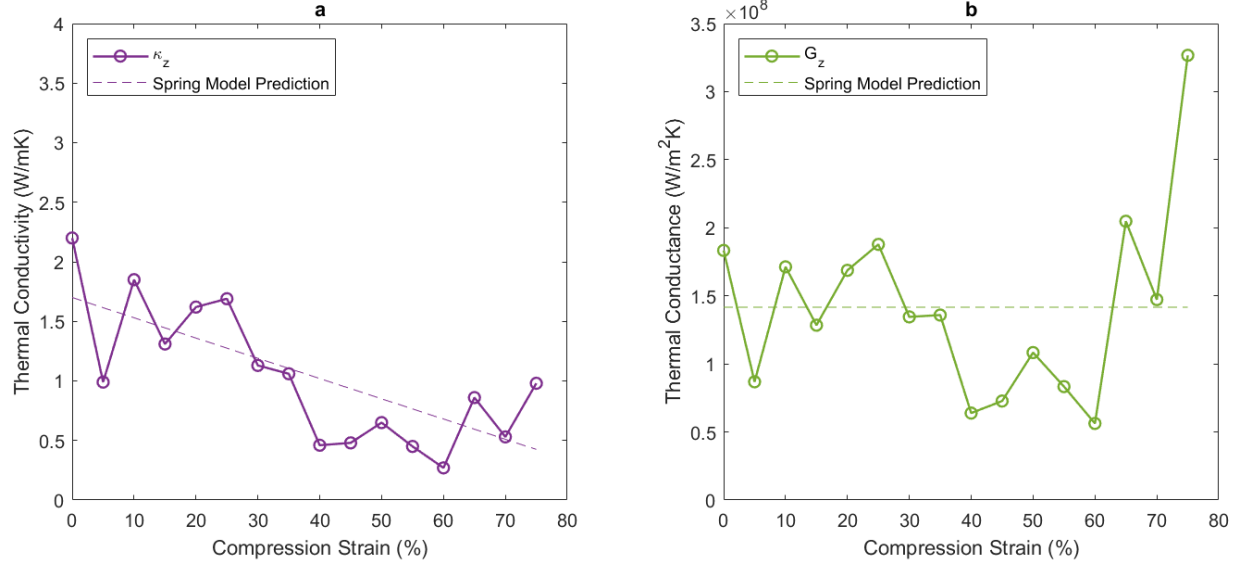


Figure 2.10: Simulation results of thermal conductivity and thermal conductance of half-density foam up to 75% compressive strain.

The decrease in thermal conductivity below 60% strain can be explained by the proposed spring model. Due to the removal of half of the atoms, branches are further apart in the foam. During early compression states, little contact has been established between branches. Hence, no new pathways are available for heat transfer. As the foam is further compressed, atoms on different branches start to involve in interactions and results in a slight increase in thermal conductivity beyond 60% strain.



### **3. FINITE ELEMENT SIMULATIONS ON CONTINUUM FOAM UNIT CELL**

The atomic scale foam structures capture the essential thermal transport physics of strain-tuning of thermal conductivity. However, their size is much smaller than the fabricated foams. Therefore, further investigation on the foam is performed on continuum level to check if constant thermal conductance occurs when ligaments are not in contact during the compression process. Based on the proposed spring model, such constant thermal conductance is because the length of the pathway heat traveled through is the same before and after compression. A decreasing thermal conductivity is also predicted due to a smaller thickness after compression. Finite element method is used to predict the thermal properties of a structure based on geometry of graphene/PDMS composite foam.

#### **3.1 The Continuum Model**

The internal structure of graphene/PDMS foam is random and nonuniform. For the benefit of FEM simulation, the representative cell is simplified and modeled as a tetrakaidecahedron frame composed by eight hexagonal and six quadrilateral faces which has been used to model graphene foam fabricated using CVD method [19] [27]. The pore size of the model is consistent with what is found in graphene/PDMS composite foam (Fig. 3.1a). The frame model is initially built in SOLIDWORKS by Weizhi Liao, a former member of this group. Since in a continuum system, spring model is not limited to certain materials, the material properties applied to perform the FEM simulations is arbitrary.

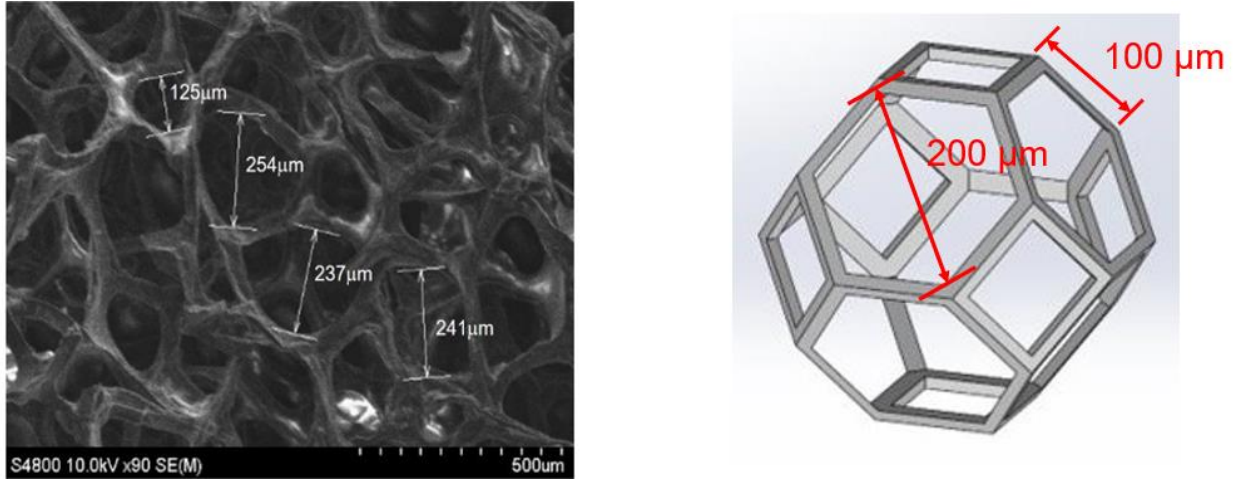


Figure 3.1: SEM picture of macroscopic graphene/PDMS composite foam (left) with pore size around 200 microns and continuum porous foam frame model (right) in SOLIDWORKS.

### 3.2 Simulation Process

Unlike MD simulation in which thermal properties can be calculated when the system is subject to a mechanical loading, available FEM tools separate mechanical and thermal simulation. Therefore, the original model is first compressed to desired thickness in a mechanical simulation. The deformed model is then saved and exported as a new model. Note that the deformed model produced in the mechanical simulation has internal stress due to strain by compression. The exported deformed model with the same strain, however, does not require any external pressure to restrain its geometry. Since the continuum model is used to validate the spring model, the effect of internal stress due to strain on thermal performance is out of our scope. Therefore, reusing the exported deformed model in thermal simulation is acceptable in this study.

#### 3.2.1 Mechanical Simulation

In the mechanical simulation of compression, the bottom surface of the model is fixed while a prescribed displacement is assigned to the top surface (Fig. 3.2). Based on observation of the compression process on graphene/PDMS foam, the lateral deformation is minimal compared with that in the loading direction. The four surfaces on the side are defined as symmetric plane such that a replicate appears on the other side and produces equal and opposite force on the surface of contact due to load from the top surface. Since the mechanical properties of graphene/PDMS foam have not been measured or reported, and the mechanical behavior of the model under compressive

load is not the focus of this study, aluminum alloy is assigned as the material of the model. The deformed model is exported and re-imported for thermal simulation.

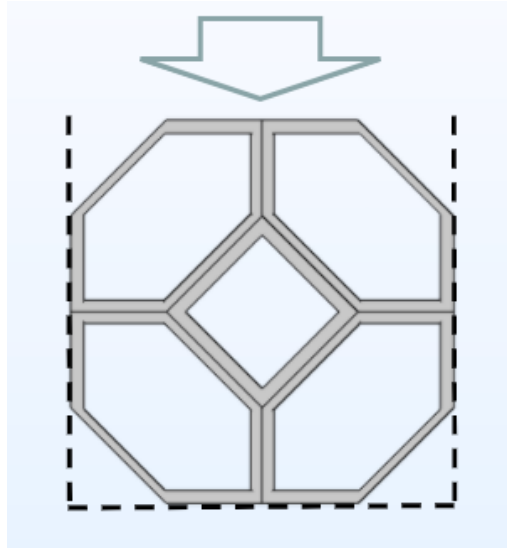


Figure 3.2: Boundary conditions for mechanical simulation.

The simulation is first performed in SOLIDWORKS. The model after exporting, however, differs from the deformed results obtained. A local shrink in cross-section area of the ligament is observed in exported model, shown in Fig. 3.3. It is caused by the mechanism SOLIDWORKS uses to export models. When exporting deformed model, SOLIDWORKS creates a cloud of points to represent each surface in the model. From the cloud of points, the deformed surface geometry is created. The total number of points and points assigned to each surface are automatically determined and cannot be manually defined by user. The surfaces obtained from the cloud of points are then “sewed” together to create the deformed solid model. Simple and less distorted geometry output a model in better shape. Highly deformed surfaces with insufficient number of points of representation results in errors such as point connection, surface geometry, unable to create deformed solid model, etc.. To increase the number of points assigned to a complex surface, such surface is split into several small surfaces to simplify geometry. The local narrowing of ligament is less significant with more split planes added (Fig. 3.4). However, the deformation of ligament is discontinuous across split plane, shown in the case of 3 split planes. The split ligament sections are sewed together at split planes and deformation of each section is calculated separately. The geometry of the model is changed by adding split planes. Another issue with split plane approach is shown in the case of 9 planes: if the split plane is at or near the location of large deformation,

the exported surface geometry will be distorted or collapsed. Hence, alternative simulation tool with better exporting solution needs to be considered.

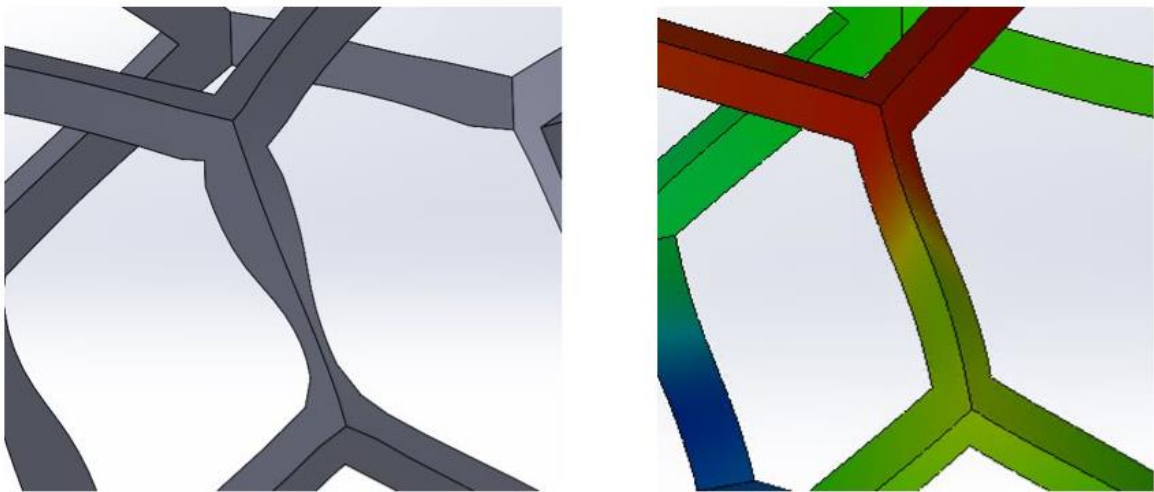


Figure 3.3: Comparison between exported model (left) and deformation result (right).

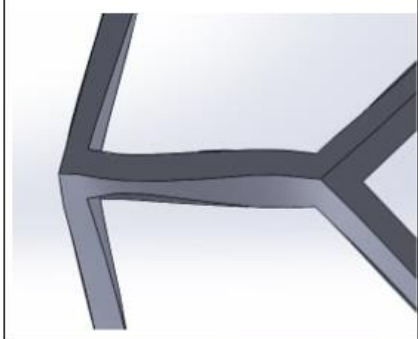
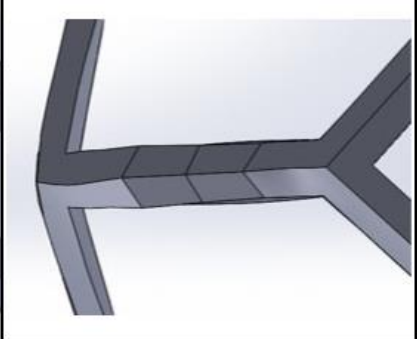
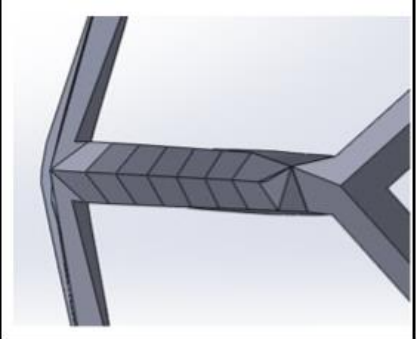
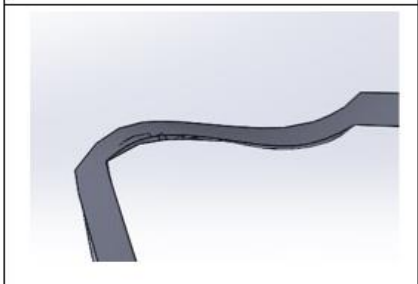
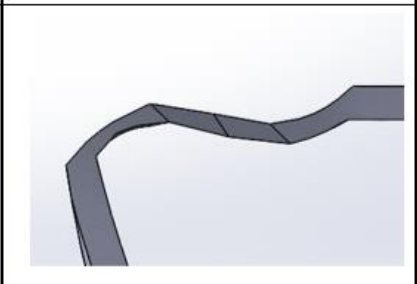
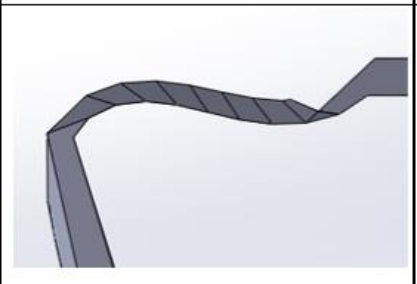
Non-split	3 split planes	9 split planes
		
		

Figure 3.4: Comparison between exported model with 0, 3, and 9 split planes.

In COMSOL Multi-physics, a deformed model can be exported in Structural Mechanics Module without any observable distortion or error in geometry. The side view of deformed model

with five different strains is shown in Fig. 3.5. The re-imported model is then re-meshed for thermal simulation.

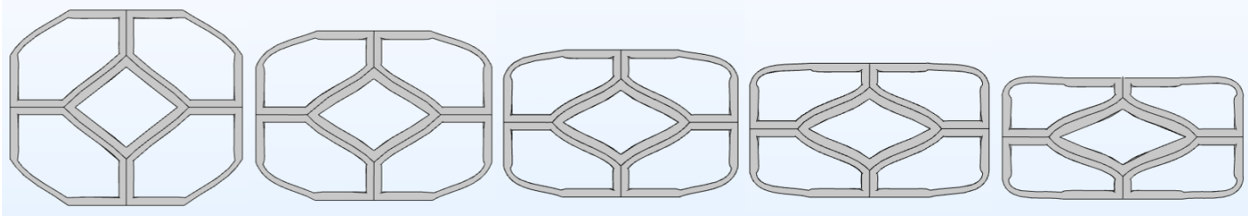


Figure 3.5: Side view of exported deformed model with different strain.

### 3.2.2 Thermal Simulation

The thermal conductivity is calculated based on Fourier's Law, by:

$$q'' = -k\nabla T, \quad (3.1)$$

where  $q''$  is the heat flux,  $k$  is the thermal conductivity, and  $\nabla T$  is the temperature gradient. In this work, only the cross-plane thermal conductivity is calculated, and the temperature gradient is obtained by finding the temperature difference between top and bottom surface. As shown in Fig. 3.6, the bottom surface of the model is fixed at 300 K and a heat flux of  $80 \text{ kWm}^{-2}$  is applied at the top surface. No radiation or convection condition is assigned to the system. The temperature gradient obtained is shown in Fig. 3.7 as an example.

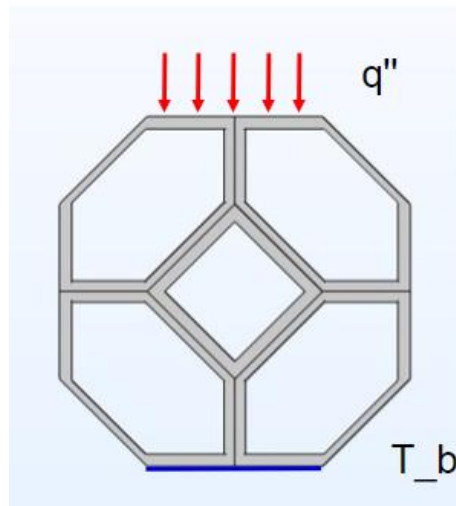


Figure 3.6: Thermal boundary loading.

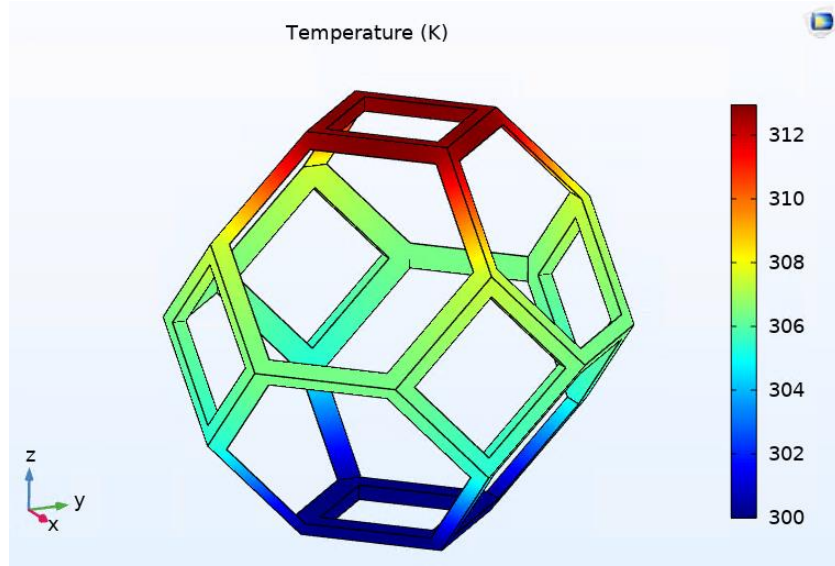


Figure 3.7: Temperature gradient obtained in thermal simulation on uncompressed frame model.

### 3.3 Results

The spring model predicts a constant thermal conductance and linearly decreased thermal conductivity with strain of a compressed system without ligament contact. The smallest thickness the model can achieve before ligaments contact occurs is around half of the original thickness. The steady state thermal simulation is performed, and the thermal conductance and conductivity results are plotted in Fig. 3.8 with prediction based on spring model. Since the material properties applied in the simulation is not those of graphene/PDMS foam, the calculated values do not correctly depict the thermal behavior of the actual foam. The normalized properties are displayed instead, defining the properties at the uncompressed state as the benchmark.

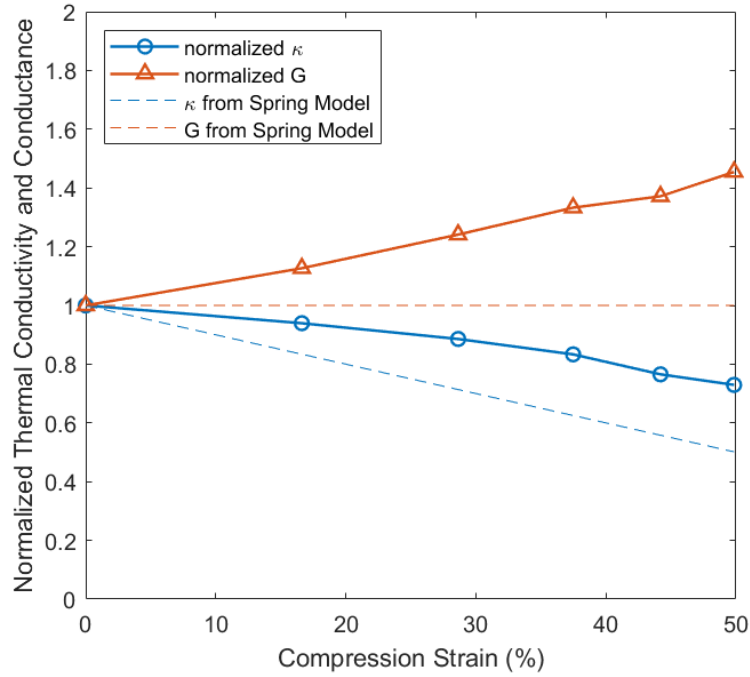


Figure 3.8: Simulation results with spring model prediction.

The simulation results display a decreasing trend in thermal conductivity as expected. The amount decreased from uncompressed state, however, is less than spring model prediction. An increase in thermal conductance is also observed. It could be due to the deformation of the frame during compression that the thickness and length of the ligament have changed, resulting in variation in thermal conductance. A small increase in the total volume of the model is observed with increasing compression strain, up to 6% at 50% strain. Since the model is under compression, the length of the ligament tends to shrink and thickness of the ligament will increase with larger volume. It results a wider thermal pathway with less resistance. Hence, a slight increase in calculated thermal conductance.

## 4. MEASUREMENTS OF VARIABLE THERMAL CONDUCTIVITY AND CONDUCTANCE OF GRAPHENE/PDMS COMPOSITE FOAM

While Molecular dynamic simulation provides an insight on behavior of thermal properties of compressible graphene-based nano-foam in microscale, the relation between strain and thermal conductivity is also directly measured in macroscale compressible foams. Even though the MD model is composed with only carbon atoms, the pure graphene foam purchased from manufacturer is very brittle. It can be compressed to less than 5% of its original thickness easily but cannot restore its shape when the applied load is reduced. The graphene/PDMS composite foam, on the other hand, has a smaller maximum strain that can be achieved on the available apparatus but restores its thickness quickly with decreasing load. The foam has a CVD grown graphene foam core embedded with polydimethylsiloxane (PDMS) which increase the elasticity of the composite foam. Its structure is shown in the SEM photo in Fig. 4.1. It has an average pore size around 200 microns and a nominal mass density of  $0.085 \text{ g/cm}^3$ . On the experiment apparatus, the foam can be compressed from its original thickness of  $\sim 1.4 \text{ mm}$  to  $\sim 0.7 \text{ mm}$  with maximum possible strain of 50%.

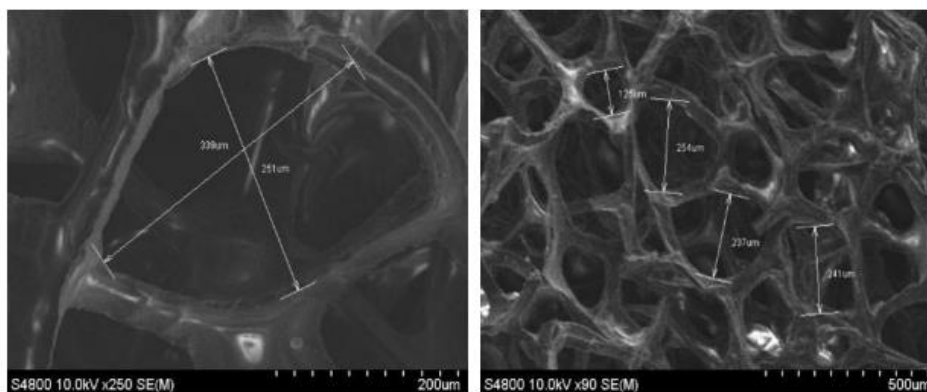


Figure 4.1: SEM photos of graphene/PDMS flexible foam.

### 4.1 Experimental Setup

The thermal conductivity of graphene/PDMS foam is determined by a method based on ASTM D5470 standard. The temperature profile is captured by the QFI MWIR-1024 high-resolution infrared microscope shown in Fig. 4.2a. Below the microscope is the cross-plane rig that holds the sample and applies a heat current. A closer view with more details is in Fig. 4.2b.



The sample (black) is sandwiched between two reference material (white) (Fig. 4.2c) and mounted between two aluminum blocks with a square cross-section of  $1\text{ cm}^2$  which is fixed on the left-hand side and has translational movement on the right controlled by a micrometer.

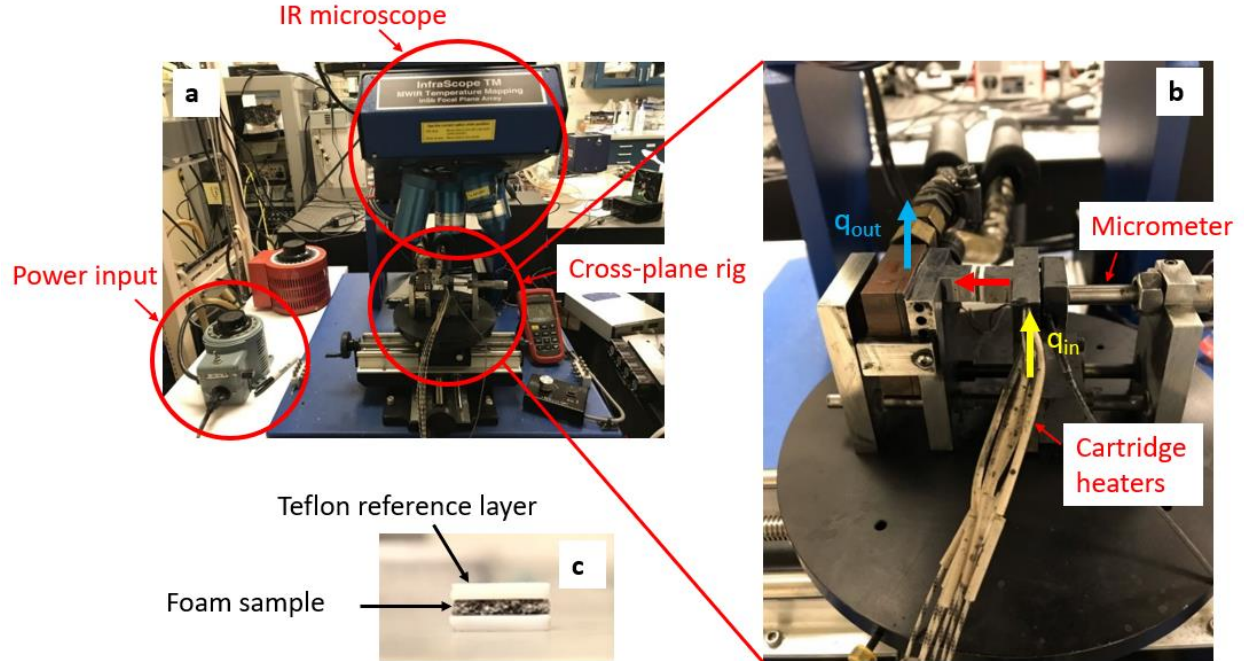


Figure 4.2: (a)(b) Experiment setup and (c) sandwiched sample.

To match the aluminum blocks, the reference material and sample are cut into  $1\text{ cm}$  by  $1\text{ cm}$  squares. The reference material is Teflon with thermal conductivity of  $0.25\text{ Wm}^{-1}\text{K}^{-1}$ . There is no thermal interface material used on the contact surfaces between the aluminum block and reference layer, and reference layer and the sample. The load that compresses the sample is applied by the micrometer. The translating aluminum block moves uniaxially, and the reference layers have flat and smooth surface. Therefore, uniform axial loading is assumed to be applied across the entire area of the foam sample. The fixed aluminum block on the left is cooled by liquid at specified temperature and the right side is heated by three cartridge heaters with controlled power input. There are two thermocouples attached on the aluminum frame right below the blocks in the center for purpose of reference and calibration.

## 4.2 Measuring Procedure

The graphene/PDMS foam has an initial thickness of 1.46 mm. Since a small amount of pressure is applied to induce enough friction to keep the sandwich structure in place, at uncompressed state, the foam has a thickness of 1.42 mm. By testing, the minimum thickness can be achieved on this apparatus is 0.71 mm and is considered as the fully compressed state. Three equally spaced intermediate states are determined at 1.24 mm, 1.06 mm, and 0.88 mm. The liquid cooled heat sink is maintained at 37 °C while the heater operates at three different power levels. Three temperature profiles are collected, and the average calculated thermal conductivity is reported as the thermal conductivity with certain compressive strain. The power input for the cartridge heater is first adjusted such that the thermal couples attached to the cold and hot aluminum block gives the same temperature reading at steady state. The criterion for steady state is that if the reading changes within 0.5 °C in 5 min. The microscope lens is then moved in position and adjusted for best focus. During the test runs, it is observed that at smaller thickness states, the foam is squeezed slightly above the level of the top surface of the reference layers. There are even some places where the foam overlaps the reference layer. Since the 1D temperature profile is obtained by averaging the 2D temperature map captured by IR microscope in in-plane direction, the overlapping of the foam results in inaccurate average temperature near the interface and causes significant calculation error in thermal conductivity. To avoid such issue, the foam sample is placed slightly below the reference layers, just enough to keep a clean interface at small thicknesses. An IR microscope focus image is shown in Fig. 4.3a. Due to the random porous structure of the foam and different top surface levels of the foam and reference layers, they cannot be in focus at the same time. The lens position is adjusted such that most foam ligaments in the view is in focus and two interfaces between foam and reference layers can be easily determined. After the microscope focus, the emissivity map is calibrated to obtain equal and constant emissivity on two reference layers by carefully adjust the power input to the heater. Since two reference layers are the same material, when their emissivity is equal, they are at the same temperature. Hence, the sandwich system is at equilibrium. It is observed in this stage that there are grains on reference layers formed when they are cut by razor blades. To obtain a more uniform emissivity map, top surfaces of reference layers are polished using sandpaper. A sample calibrated emissivity map is shown in Fig. 4.3b. The plot in the smaller window is the emissivity measurement on the horizontal

white dash line across the sandwich structure. After calibration, the power input is then increased to higher levels. The temperature map in Fig. 4.3c is collected at steady state for all power levels.

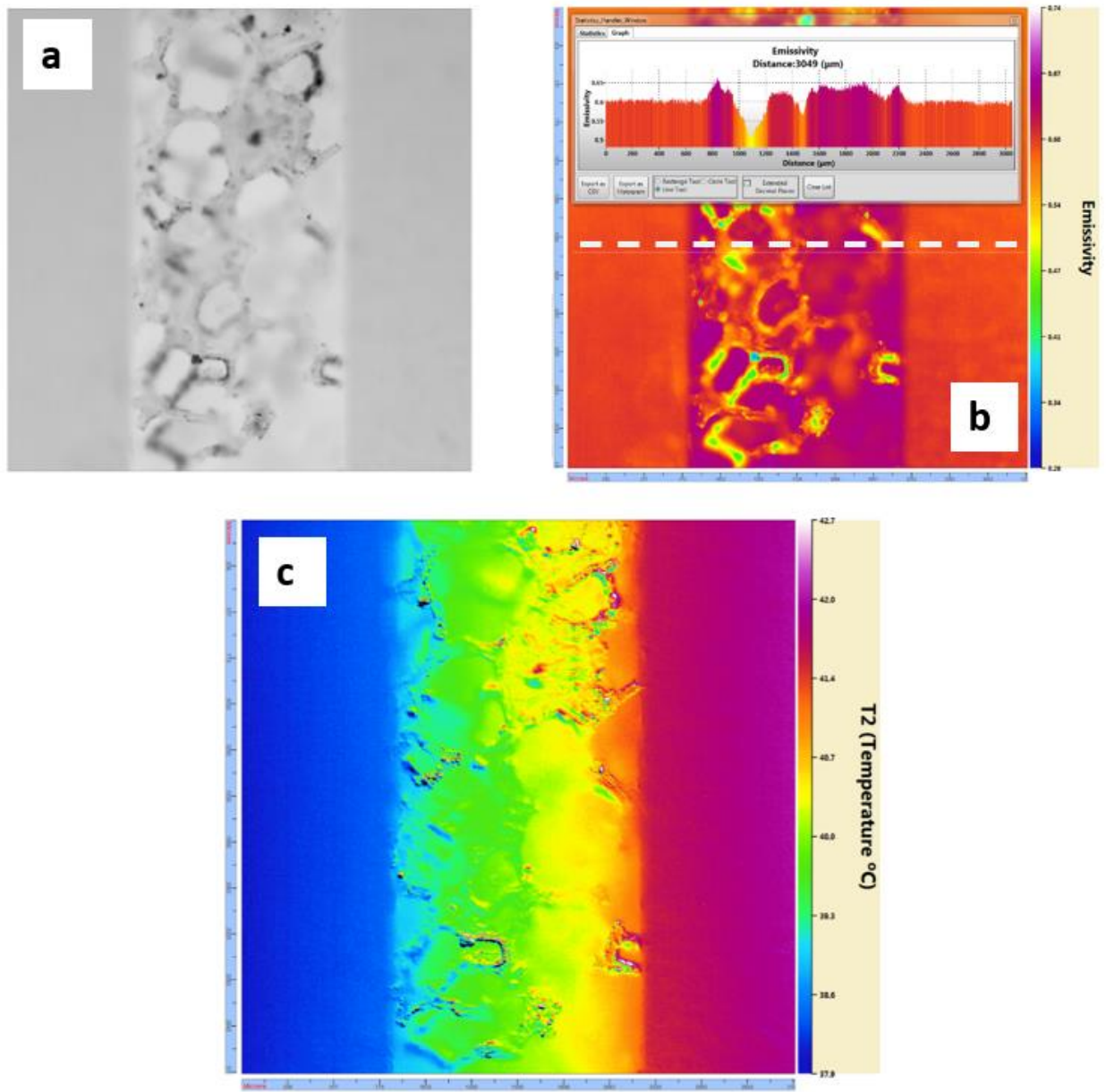


Figure 4.3: (a) IR microscope focus image, (b) emissivity calibration map, and (c) temperature map.

The thickness of the foam and reference layers are relatively small compared to their cross-section length. Convective heat loss through the side surfaces can be observed but not significant. To eliminate convective heat loss effect on the temperature map, 4x lens is used and only captures the middle 1/3 portion of the sandwiched sample.

### 4.3 Results

The 2D temperature map captured by the IR microscope is analyzed using a MATLAB code. The temperature image is first rotated such that the sandwich structure is perfectly horizontal. The temperature data on the same level horizontally are averaged to plot a 1D temperature profile in the cross-plane direction (Fig. 4.4). The reference material has flat and smooth surface, so the temperature profile is linear till the interface region. The heat flux through the sandwich structure is calculated based on the slope of the temperature profile in the reference material region and the manually input thermal conductivity of the reference material:

$$q = -k_{ref} \left. \frac{dT}{dx} \right|_{ref}. \quad (4.1)$$

The foam has a random porous geometry and an uneven surface. Therefore, its temperature profile is in a noisy shape. The value for the foam is calculated by applying a linear fitting over the temperature profile across the foam thickness. The heat flux obtained from the reference material is used to determine the thermal conductivity of the foam:

$$k_{foam} = -\frac{q}{\left. \frac{dT}{dx} \right|_{foam}} = \frac{k_{ref} \left. \frac{dT}{dx} \right|_{ref}}{\left. \frac{dT}{dx} \right|_{foam}}, \quad (4.2)$$

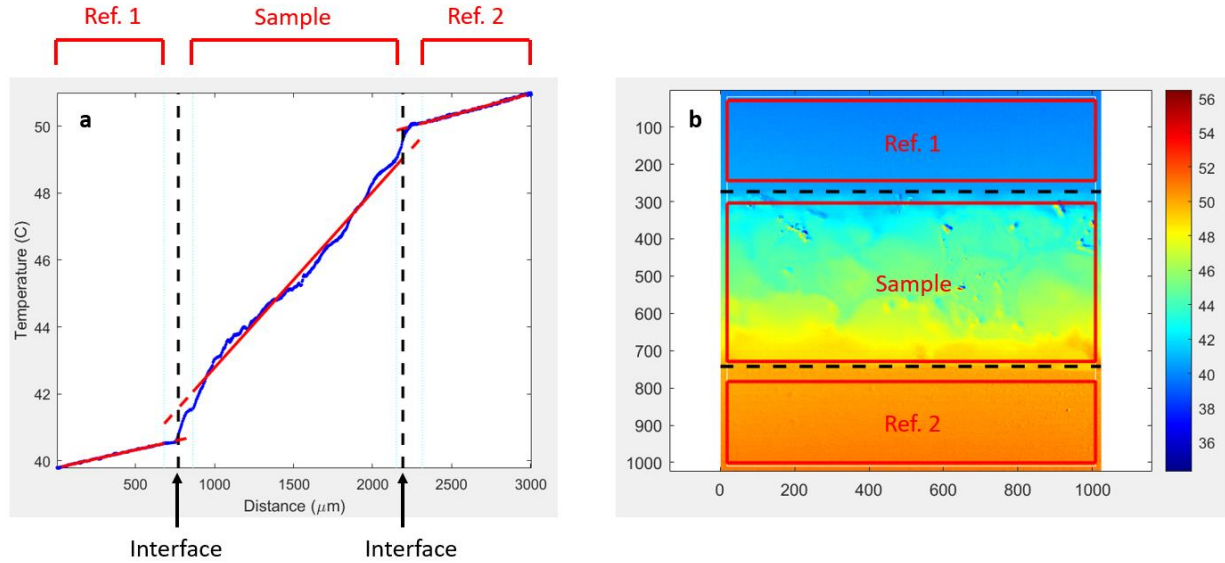


Figure 4.4: (a) 1D temperature profile and (b) 2D temperature map with corresponding regions.

The total temperature drop across the sample with different applied heat flux at 5 compression levels is plotted in Fig. 4.5. It can serve as a tuning map for thermal switch/regulator

that is designed using this graphene/PDMS foam. For instance, if a constant heat flux of  $400\text{W/m}^2$  is across the system, there are 5 options in temperature drop based on selected foam thickness: it can be as high as  $7.5\text{ K}$  at  $1.42\text{ mm}$ , or as low as  $1.5\text{ K}$  at  $0.71\text{ mm}$ . Similarly, a constant temperature drop can be maintained with different heat flux by varying the thickness.

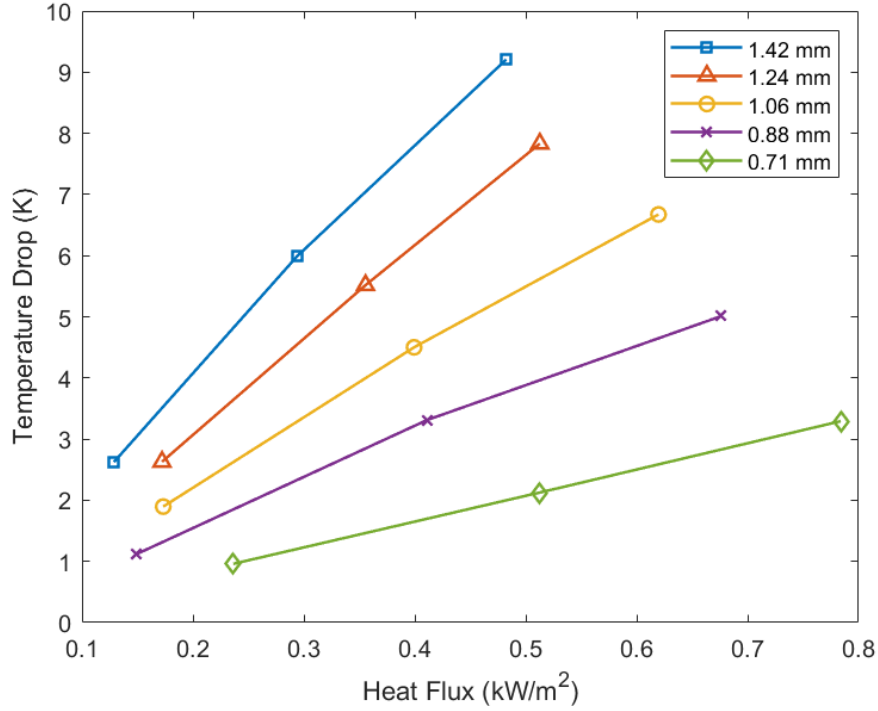


Figure 4.5: Temperature drop at various heat flux of foam with different thicknesses.

The variation in thermal conductivity with increasing strain is shown in Fig. 4.6. The uncertainty in measurements is influenced by several factors. The calibrated temperature at system equilibrium may have small offset between reference layers as the emissivity plot is not entirely uniform. The thermal conductivity of reference material may differ from reported value by 10%. There is also human error introduced when selecting reference and sample regions in data analysis. By shifting the selection box by several pixels at a time, the uncertainty in heat flux and temperature drop is obtained. The combined total error is calculated using uncertainty propagation. An increasing trend is observed with increasing strain. As the foam is compressed, ligaments in the foam are in contact, creating more thermal transport path for more efficient heat transfer. With higher pressure applied to the foam, the contact resistance between touching ligaments is reduced, and therefore, enhances thermal conductivity of the foam. The measured properties are more

sensitive to strain at higher level, which is also found in MD simulation. The spring model prediction, however, is not found in graphene/PDMS foam, since there are many internal contacts occurring at the smallest measured strain and the strain small enough to observe spring model prediction cannot be achieved due to accuracy of strain measurement.

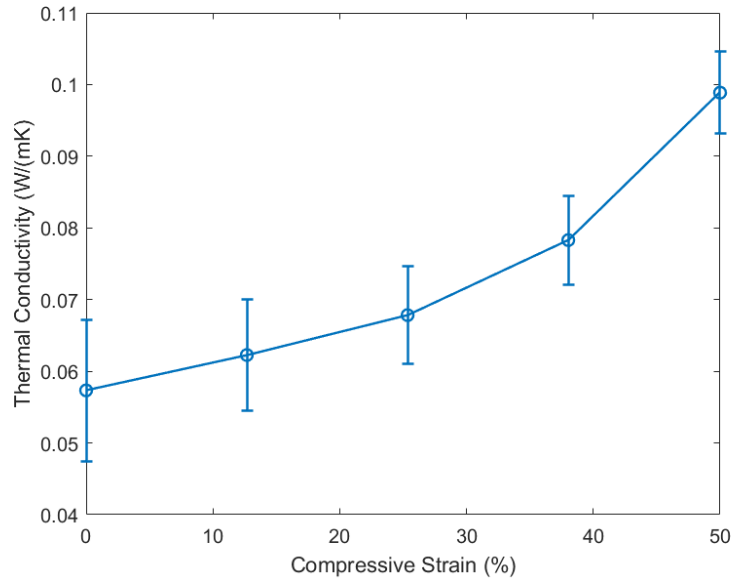


Figure 4.6: Variation of thermal conductivity of graphene/PDMS foam with compressive strain.

## 5. CONCLUSION AND FUTURE WORK

Thermal behavior of compressible graphene-based foams has been studied on three systems with different dimensions, from nanoscale to macroscale. MD simulations show an increase in thermal conductivity at high compression strain due to enhanced thermal transport in internal contact and a decrease governed by spring model when the length and number of thermal pathway remain relatively constant at low compression level. The spring model prediction is effective for a higher strain in foam with lower initial mass density at uncompressed state. In a continuum model with similar geometry as graphene/PDMS composite foam, a decrease in thermal conductivity is observed but displays deviation from spring model prediction due to deformed ligaments. The increase in both thermal conductance and conductivity is measured in flexible graphene/PDMS foam using an IR microscope. The properties are more sensitive to strain at higher compression level, which agrees with MD simulation results.

Beyond the scope of this work, the effect of ligament contact on thermal transport in the continuum model can be investigated. The structure of macroscopic compressible foam can be designed to reach greater switching ratio by increasing ligament contact and reducing contact resistance. The enhancement of thermal properties of free-standing compressible media should also be considered to help elevating the maximum value can be achieved.

## 6. REFERENCES

- [1] A. Pesaran, "Battery thermal models for hybrid vehicle simulations," *J Power Sources*, vol. 110, pp. 337-382, 2002.
- [2] N. Sata, "Thermal Behavior analysis of lithium-ion batteries for electric and hybrid vehicles," *J Power Sources*, vol. 99, pp. 70-77, 2001.
- [3] S. Khateeb, S. Amiruddin, M. Farid, J. Sleman and S. Al-Hallaj, "Thermal management of Li-ion battery with phase change material for electric scooter: experiment validation," *J Power Sources*, vol. 142, pp. 345-353, 2005.
- [4] G. Nagasubramanian, "Electric characteristics of 18650 Li-ion cells at low temperatures," *J Appl Electrochem*, vol. 31, pp. 99-104, 2001.
- [5] Q. Wang, B. Jiang, B. Li and Y. Yan, "A critical review of thermal management models and solutions of lithium-ion batteries for the development of pure electric vehicles," *Renewable and Sustainable Energy Reviews*, vol. 64, pp. 106-128, 2016.
- [6] J. Cho, T. Wiser, C. Richards, D. Bahr and R. Richards, "Fabrication and characterization of a thermal switch," *Sensors and Actuators A*, vol. 133, pp. 55-63, 2007.
- [7] W. Gu, G.-H. Tang and W.-Q. Tao, "Thermal switch and thermal rectification enabled by near-field radiative heat transfer between three slabs," *International Journal of Heat and Mass Transfer*, vol. 82, pp. 429-434, 2015.
- [8] T. Yang, B. Kwon, P. B. Weisensee, Jin Gu Kang, X. Li, P. Braun, N. Miljkovic and W. P. King, "Millimeter-scale liquid metal droplet thermal switch," *Applied Physics Letters*, vol. 112, p. 063505, 2018.



- [9] M. Hao, J. Li, S. Park, S. Moura and C. Dames, "Efficient thermal management of Li-ion batteries with a passive interfacial thermal regulator based on a shape memory alloy," *Nature Energy*, vol. 3, pp. 899-906, 2018.
- [10] J. A. Tomko, A. Pena-Francesch, H. Jung, M. Tyagi, B. D. Allen, M. C. Demirel and P. E. Hopkins, "Tunable thermal transport and resersible thermal conductivity switching in topologically networked bio-inspired materials," *Nature Nanotechnology*, vol. 13, pp. 959-964, 2018.
- [11] C. W. Chang, D. Okawa, H. Garcia, T. D. Yuzvinsky, A. Majumdar and A. Zetti, "Tunable thermal links," *Applied Physics Letters*, vol. 90, p. 193114, 2007.
- [12] A. A. Balandin, S. Ghosh, W. Bao, I. Calizo, D. Teweldebrhan, F. Miao and Chun Ning Lau, "Superior Thermal Conductivity of Single-layer Graphene," *Nano Letters*, vol. 8, no. 3, pp. 902-907, 2008.
- [13] S. Ghosh, I. Calizo, D. Teweldebrhan, E. P. Pokatilov, D. L. Nika, A. A. Balandin, W. Bao, F. Miao and C. N. Lau, "Extremely high thermal conductivity of graphene: Prospects for thermal management applications in nanoelectronic circuits," *Applied Physics Letters*, vol. 92, p. 151911, 2008.
- [14] Z. Chen, W. Ren, L. Gao, B. Liu, S. Pei and H.-M. Cheng, "Three-dimensional flexible and conductive interconnected graphene networks grown by chemical vapour deposition," *Nature Materials*, vol. 10, pp. 424-428, 2011.
- [15] H. Lin, S. Xu, X. Wang and N. Mei, "Significantly reduced thermal diffusivity of free-standing two-layer graphene in graphene foam," *Nanotechnology*, vol. 24, p. 415706, 2013.
- [16] Y. Wu, Z. Wang, X. Liu, X. Shen, Q. Zheng, Q. Xue and J.-K. Kim, "Ultralight Graphene Foam/Conductive Polymer Composites for Exceptional Electromagnetic Interference Shielding," *ACS Applied Materials & Interfaces*, vol. 9, no. 10, pp. 9059-9069, 2017.
- [17] Y.-H. Zhao, Z.-K. Wu and S.-L. Bai, "Study on thermal properties of graphene foam/graphene sheets filled polymer composites," *Composites: Part A*, vol. 72, pp. 200-206, 2015.

- [18] Y.-H. Zhao, Y.-F. Zhang, S.-L. Bai and X.-W. Yuan, "Carbon fibre/graphene foam/polymer composites with enhanced mechanical and thermal properties," *Composites Part B*, vol. 94, pp. 102-108, 2016.
- [19] Y.-H. Zhao, Y.-F. Zhang and S.-L. Bai, "High thermal conductivity of flexible polymer composites due to synergistic effect of multilayer graphene flakes and graphene foam," *Composites: Part A*, vol. 85, pp. 148-155, 2016.
- [20] S. Plimpton, "Fast Parallel Algorithms for Short-Range Molecular Dynamics," *Journal of Computational Physics*, vol. 117, no. 1, pp. 1-19, 1995.
- [21] A. Pedrielli, S. Taioli, G. Garberoglio and N. M. Pugno, "Mechanical and thermal properties of graphene random nanofoams via Molecular Dynamics simulations," *Carbon*, vol. 132, pp. 766-775, 2018.
- [22] W. Humphrey, A. Dalke and K. Schulten, "VMD: Visual molecular dynamics," *Journal of Molecular Graphics*, vol. 14, no. 1, pp. 33-38, 1996.
- [23] M. S. Green, "Markoff Random Processes and the Statistical Mechanics of Time-Dependent Phenomena. II. Irreversible Processes in Fluids," *Journal of Chemical Physics*, vol. 22, p. 398, 1954.
- [24] R. Kubo, "Statistical-Mechanical Theory of Irreversible Processes. I. General Theory and Simple Applications to Magnetic and Conduction Problems," *Journal of the Physical Society of Japan*, vol. 12, pp. 570-586, 1957.
- [25] J. Tersoff, "Empirical Interatomic Potential for Carbon, with Applications to Amorphous Carbon," *Physical Review Letters*, vol. 61, p. 2879, 1988.
- [26] M. Li, Y. Sun, H. Xiao, X. Hu and Y. Yue, "High temperature dependence of thermal transport in graphene foam," *Nanotechnology*, vol. 26, p. 105703, 2015.
- [27] Y.-F. Zhang, Y.-H. Zhao, S.-L. Bai and X. Yuan, "Numerical simulation of thermal conductivity of graphene filled polymer composites," *Composites Part B*, vol. 106, pp. 324-331, 2016.